JACS
JOURNAL OF THE AMERICAN CHEMICAL SOCIETY

Article

pubs.acs.org/JACS

Unveiling the Role of *Hot* Charge-Transfer States in Molecular Aggregates via Nonadiabatic Dynamics

Daniele Fazzi,*[,†] Mario Barbatti,*[,‡] and Walter Thiel*[,†]

[†]Max-Planck-Institut für Kohlenforschung, Kaiser-Wilhelm-Platz 1, D-45470 Mülheim an der Ruhr, Germany

[‡]Aix Marseille Université, CNRS, ICR UMR7273, 13397 Marseille, France

Supporting Information

ABSTRACT: Exciton dynamics governs energy transfer and charge generation in organic functional materials. We investigate high-energy nonadiabatic excited-state dynamics for a bithiophene dimer to describe time-dependent excitonic effects in molecular aggregates. We show that the lowest excited states are populated on the subpicosecond time scale. These states are localized and unproductive in terms of charge separation. Productive high-energy charge-transfer (CT) states are populated within 50 fs during exciton deactivation, but they are short-lived (~100 fs) and quickly transfer their population to lower states. Our simulations offer molecular-level insights into ultrafast photoinduced charge separation potentially triggered by *hot* CT states in solid-state organic materials. Design rules are suggested to increase *hot* exciton lifetimes, favoring the population of CT states as gateways for direct charge generation. These rules may boost the CT quantum yield by depleting unproductive recombination channels.

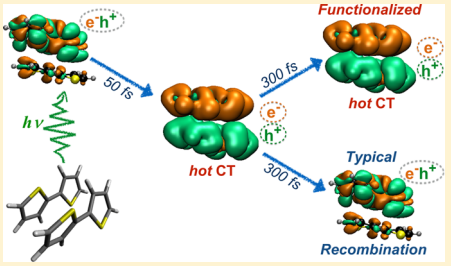

INTRODUCTION

Excitons are the primary outcome of light−matter interactions. Their formation and relaxation play a key role in a variety of areas, including chemical reaction dynamics,[1] ultrafast electron-nuclei processes in organic and inorganic materials,[2−4] dynamics of semiconductors and quantum dots,[5] and light harvesting and energy transfer in photosynthetic systems.[6] In particular, ultrafast exciton dynamics governs the energy flow and the charge generation/recombination mechanisms in organic π-electron conjugated materials and interfaces.[7]

In the last two decades, our understanding of ultrafast phenomena ruling exciton dynamics and charge generation processes in organic materials has significantly improved. This progress took place in the wake of scientific and industrial developments in photovoltaics, electronics, spintronics, and thermoelectrics, with strong focus on *soft* materials.[8−15]

However, several features of exciton and charge generation dynamics at the molecular scale are still obscure. The usage of fairly simple concepts such as *frontier orbitals* and *interfacial states* is still common in the literature. Even the role of one of the primary process, the high-energy (*hot*) exciton relaxation, is still under debate[16−20] in the organic and hybrid photovoltaics communities: it is unclear whether *hot* excitons would favor an *instantaneous* electron−hole charge separation, thus increasing the overall charge generation efficiency, or alternatively lead to unproductive nonradiative decay toward low-lying electron−hole bound states.

Experimental evidence of fast (~30−100 fs) electron transfer processes and polaron formation from photoinduced *hot* excitons has recently been reported for thiophene-based molecules,[21] acenes,[22] diverse polymers,[23] and polymer/fullerene interfaces.[17,18,21,24−26] This ultrafast population of *hot* CT states competes with nonradiative mechanisms within the manifold of excited states.[27] Internal relaxation can bring *hot* excitons to the bottom of the excited-state band, thus reducing the lifetime of *hot* CTs and allowing for nonradiative pathways and recombination processes that are detrimental for efficient charge generation.[28]

An appropriate theoretical description and modeling of ultrafast exciton relaxation in organic aggregates is urgently needed.[29,30] Pioneering recent studies by Rossky et al.,[31,32] Tamura et al.,[33,34] Tretiak et al.,[4,13,35] and Prezhdo et al.[10,36,37] describe the nonadiabatic excited-state dynamics of medium-sized systems based on different approximations. Limited to model Hamiltonians, single-determinant Kohn−Sham treatments or low-dimensional 1-D systems, these simulations have contributed to the understanding of the dynamic processes, but without addressing in detail the nature of the electronic states accessed during the relaxation process. This knowledge gap is tackled in our present work.

To understand ultrafast exciton relaxation phenomena and the population of *hot* CT states from an atomistic and time-dependent viewpoint, we have performed *full-dimensional* nonadiabatic excited-state dynamics simulations based on linear-response time-dependent density functional theory (TDDFT)[29,38] for the bithiophene stacking dimer (Figure 1), a molecular aggregate representative of a large class of solid-state organic π-conjugated materials. Our aim is to understand how *hot* excitons relax and whether we can control their lifetime. For this purpose, we use nonadiabatic excited-state dynamics to understand and predict (i) the excited-state

Received: December 24, 2015
Published: March 11, 2016

DOI: 10.1021/jacs.5b13210
J. Am. Chem. Soc. 2016, 138, 4502−4511

relaxation time scales for high-energy excitations; (ii) the interplay between inter- and intramolecular nonadiabatic relaxations; (iii) the population of CT states; (iv) exciton delocalization/localization processes; and (v) the nuclear vibrations governing exciton dynamics in thiophene-based molecular aggregates.

Our working hypothesis is that productive charge separation and transfer processes in organic electronics and photovoltaics depend on the population and lifetime of CT states. However, such CT states are usually not among the lowest states in the manifold of excited states in organic homo- and hetero-junctions.[39] If the lifetime of high-lying (*hot*) excited states is extended, the time the dimer spends in CT states rises, which increases the odds of productive charge separation. In this spirit, we propose a new goal for the design of functionalized molecular aggregates: if we can modify the excited-state electronic structure by introducing energy gaps between high- and low-energy bands, this will disfavor unproductive ultrafast exciton relaxation and increase the residence time of the photoexcitation on productive *hot* CTs (see Scheme 1). The main assumption underlying this hypothetical *scenario* is that charge separation is triggered by a charge transfer process between two monomers. However, it might also be possible that charge transfer states extended over several monomers act as triggers for (long-range) charge separation.[40] We do not address this possibility here, but only point out that in principle it can be studied using the same methodology.

Scheme 1[a]

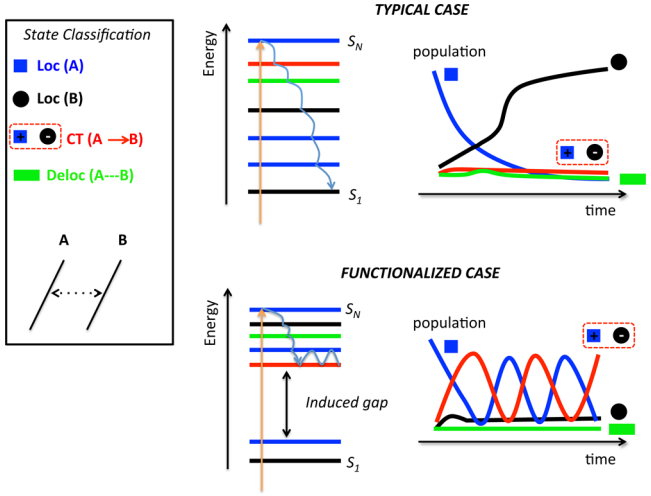

[a]Left side: color code for excited-state classification and sketch of a molecular dimer. Right side: excited-state classification and time-dependent state population of a typical (top) and a functionalized (bottom) molecular aggregate.

COMPUTATIONAL METHODS

Ground- and excited-state properties of the bithiophene dimer were investigated with DFT and TDDFT. The ground-state and the first three excited-state equilibrium geometries were optimized at the ωB97XD level, using the 6-31G*, 6-311+G*, and aug-ccpVTZ basis sets. This approach, which incorporates long-range and dispersion corrections, has been previously shown to provide semiquantitatively correct predictions for this type of systems.[39] Static calculations were done both in vacuum and in a dielectric using the conductor polarizable continuum model (CPCM). Ground-state geometries and vertical electronic transitions were also evaluated using the algebraic diagrammatic construction to second order (ADC(2)),[41] combined with SVP and def2-TZVP basis sets. Further details are given in the Supporting Information (Supplementary Note 1) including a more thorough description of the computational procedures and additional numerical results.

Absorption cross sections were computed with the nuclear ensemble method based on harmonic-oscillator Wigner distributions. These calculations employed the ωB97XD functional and the 6-31G* and 6-311+G* basis sets, both in vacuum and in a dielectric continuum (see Supporting Information). A total of 150 points were considered for spectrum generation.

Nonadiabatic excited-state dynamics were done with TDDFT using the fewest-switching surface hopping (FSSH) method as implemented in NEWTON-X interfaced with Gaussian 09.[42] Dynamics were run at the TD-ωB97XD/6-31G* level, using a microcanonical ensemble. The time step for integration of the classical equations was 0.5 fs. The integration of the quantum equations was done with 0.025 fs steps using interpolated properties between classical steps. Time-dependent coefficients were corrected for decoherence effects as described in ref 43.

The large density of states in the dimers leads to numerous state crossings. In particular, the occurrence of trivial crossings between noninteracting or weakly interacting states has been recognized as potentially challenging for FSSH. In such cases, conventional FSSH becomes costly, requiring very small time steps.[44,45] This problem has been tackled by different strategies to track down the diabatic nature of the crossings, including the local diabatization method,[46,47] the self-consistent FSSH,[45] the flexible surface hopping techninque,[48] the global flux surface hopping,[49] and the Min Cost algorithm.[44] In the present work, nonadiabatic couplings between excited states were computed from time-dependent wave function overlap integrals as proposed by Hammes-Schiffer and Tully[50] based on wave functions built through Casida's Ansatz.[51] This approach has been extensively used for computating nonadiabatic couplings in dynamics simulations[52−55] and has been found to be very stable even in the presence of trivial crossings.[47]

Due to the limitations of the linear-response TDDFT and Kohn−Sham DFT methods in providing reliable electronic states near intersections with the ground state, nonadiabatic transitions between the first excited state and the ground state were not computed. Trajectories were run for a maximum of 300 fs or until a crossing with the ground state (within 0.15 eV) was reached. In such cases, the last time step was taken to indicate internal conversion to the ground state. Under this assumption, the occupation of the ground state and the correction to the S_1 occupation were computed at each time step as reported in ref 56.

The excited states were classified as localized, delocalized, or charge-transfer using the method introduced and discussed in the literature.[39,57] In brief, the molecular aggregate is split in two units A and B (in this case, the two monomers); then, the contribution of each molecular orbital to each unit is computed with a Mulliken partition. With this information, the amount of localization ($\sum P_A^I$) and of charge transfer (ΔP_A^I) for each electronic state I is computed for unit A based on a configuration−interaction wave function approximation, using linear-response coefficients. Finally, the densities $\sum P_A^I$ and ΔP_A^I are compared to predefined thresholds to classify the states.

RESULTS AND DISCUSSION

Absorption Spectrum. The computed TDDFT vertical excitations and absorption cross sections for the bithiophene monomer and the van-der-Waals (vdW) dimer are reported in Figure 1.

Just like in other noncovalent organic dimers,[58] the ground-state structure of bithiophene dimer is asymmetric causing a split of the low-lying excited states (S_1^{AB}, S_2^{AB}). Analysis of the dimer excited states shows S_1^{AB} and S_2^{AB} to be localized within each monomer. Delocalized excited states are predicted at

DOI: 10.1021/jacs.5b13210
J. Am. Chem. Soc. 2016, 138, 4502−4511

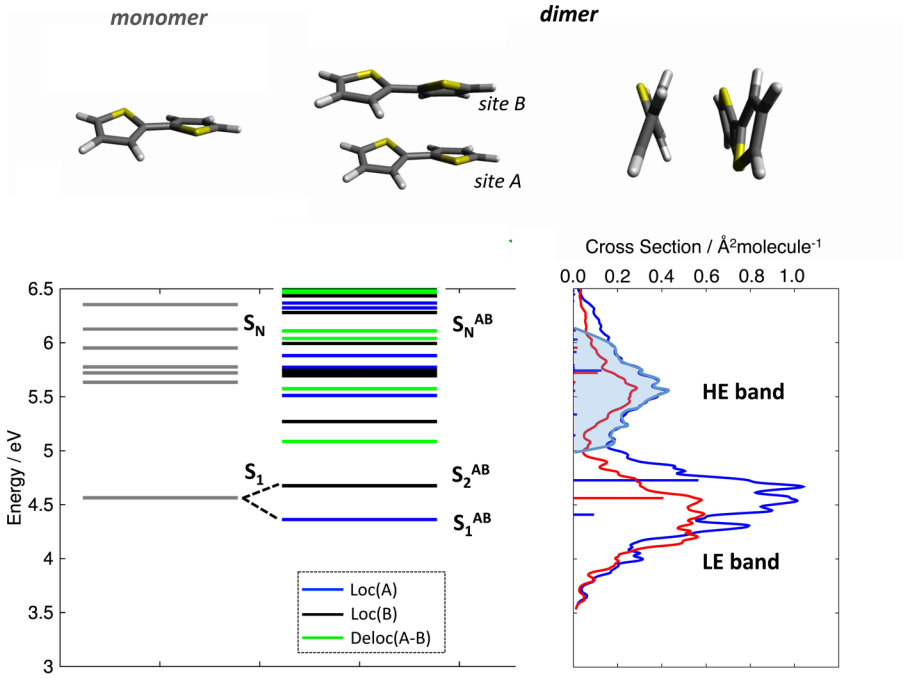

Figure 1. Top: DFT (ωB97XD/6-31G*) molecular structures for the bithiophene monomer and dimer (lateral and side views). Bottom left: TDDFT (ωB97XD/6-31G*) vertical transition energies for the bithiophene monomer and dimer, and excited-state classification. Bottom right: absorption cross sections of monomer (red) and dimer (blue), and oscillator strengths (horizontal bars); the photoexcited high-energy (HE) band is represented by the shaded area.

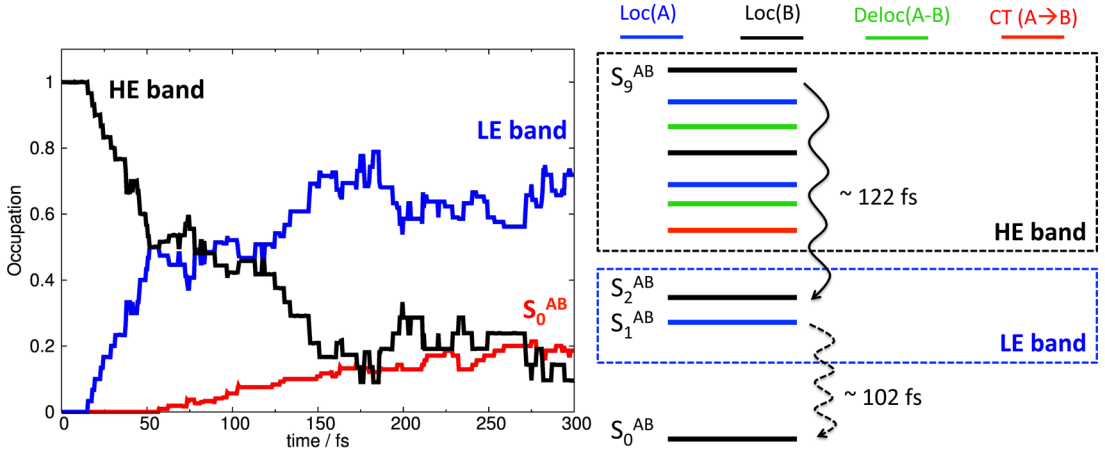

Figure 2. TDDFT (ωB97XD/6-31G*) nonadiabatic excited-state dynamics initiated by populating a high-energy excited state (S_9^{AB}). Left: state occupations vs time. Right: sketch of ultrafast relaxation within the manifold of high-energy excited states (HE band) toward the low-energy states (LE band, S_1^{AB} and S_2^{AB}) and of nonradiative relaxation to the ground state.

higher energies, and excited states with CT character are not present below 6.5 eV in the vertical spectrum. The dimer absorption cross section gives rise to two bands, one at low energy (LE, ~4.5 eV) and another at high energy (HE, ~5−6 eV). A manifold of excited states contributes to the HE band, and among them, S_8 has non-negligible oscillator strength (f = 0.13). At distorted ensemble geometries, the bright state may also occur as S_9.

High-Energy Nonadiabatic Dynamics. TDDFT nonadiabatic excited-state dynamics was initiated in the HE band, restricting the excitation to the 5.5 ± 0.5 eV spectral window (shaded area in Figure 1). A total of 30 trajectories, considering 10 coupled singlet electronic states in each case, were initiated in the S_9 state and propagated up to 300 fs or until the S_1^{AB}/S_0^{AB} gap became smaller than 0.15 eV. Six trajectories reached the S_1^{AB}/S_0^{AB} crossing during the simulations, while 24 had still large S_1^{AB}/S_0^{AB} energy gaps at 300 fs.

Figure 2 shows the occupations of the states in the HE band (sum over S_3^{AB} to S_9^{AB}) and the LE band (sum over S_1^{AB} and S_2^{AB}) and also of the S_0^{AB} ground state as a function of time. The HE band starts to transfer population to LE after 15 fs. Its population decays exponentially with a time constant of 122 fs. The LE band transfers about 20% of the population to the ground state, with a time constant of 102 fs (see Supplementary Note 2).

These findings can be compared to very recent TDDFT[56] and ADC(2)[59] nonadiabatic excited-state dynamics performed on an isolated bithiophene monomer. In this case, HE-band excitation leads to over 80% occupation of S_0 within 300 fs, while for the dimer, the fraction is only 19%. Therefore, the

DOI: 10.1021/jacs.5b13210
J. Am. Chem. Soc. 2016, 138, 4502−4511

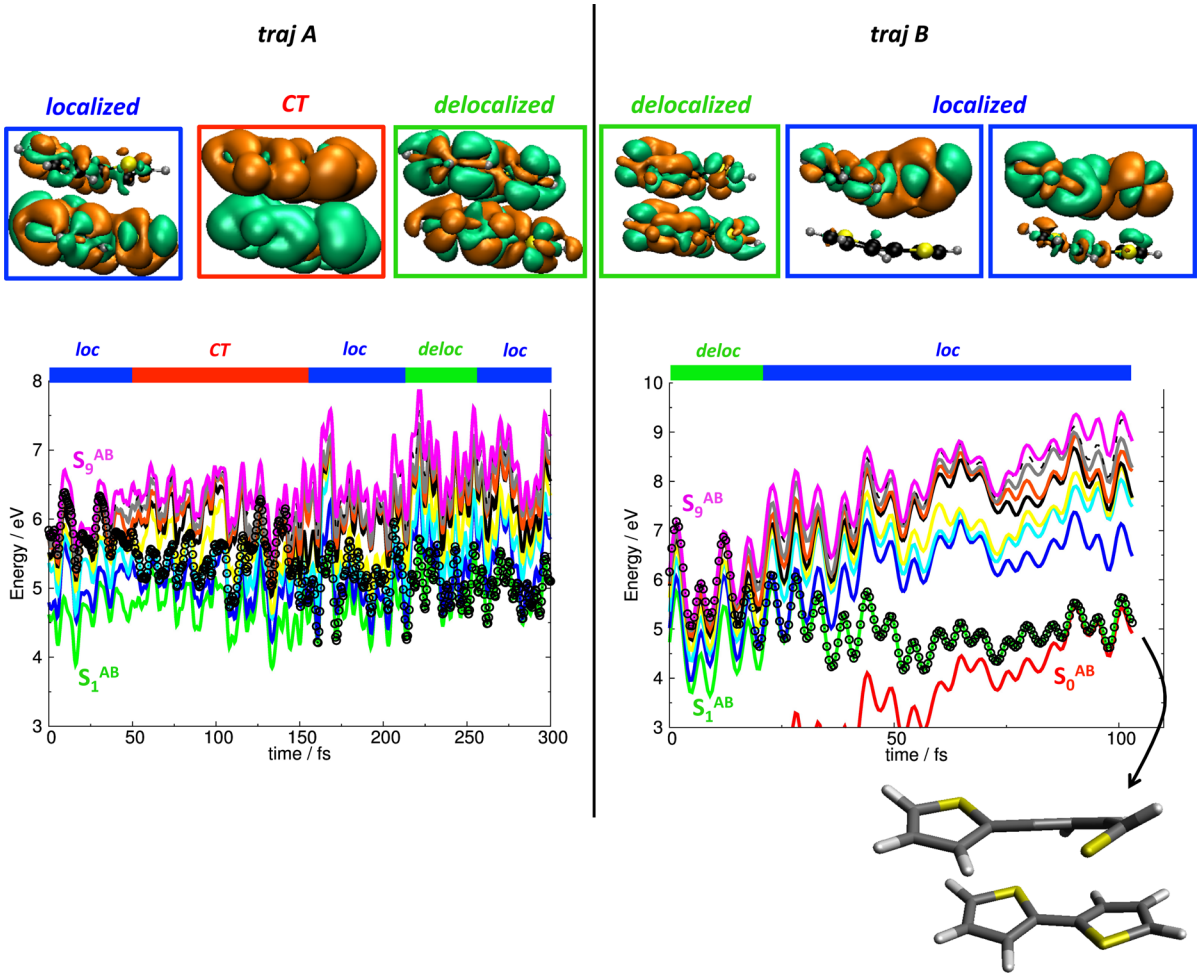

Figure 3. Two exemplary trajectories: left side, traj A, t = 0−300 fs; right side, traj B, t = 0−100 fs. Top: snapshots of the electronic-density difference between the occupied excited state and the ground state for typical localized (*loc*), delocalized (*deloc*), or CT states; orange/green regions indicate loss/gain of electron density upon excitation. Bottom: time evolution of the excited-state energies (TD-ωB97XD/6-31G*) with indication of the prevailing state character. Also shown is the molecular structure close to the S_1^{AB}/S_0^{AB} intersection seam featuring the typical thiophene ring opening.

ultrafast nonradiative decay through S_1/S_0 crossing is significantly delayed in the vdW dimer compared to the monomer.

To better understand the exciton dynamics and the transfer processes in the dimer, two exemplary trajectories are illustrated in Figure 3. Traj A is representative of those remaining in the excited-state manifold during the entire simulation, while traj B is an example of those few that reach the S_1/S_0 crossing before 300 fs.

In traj A, the photoexcited dimer decays from a high-energy excited state (S_9^{AB}) to the low-lying S_2^{AB} and S_1^{AB} states in 150 fs. Thereafter, the dynamics continues in the LE regime and does not reach the ground state. In traj B, the photoexcited system relaxes from S_9^{AB} to S_1^{AB} in ∼30 fs and arrives at the S_1^{AB}/S_0^{AB} intersection seam in about 100 fs.

To gain insight into the different deactivation mechanisms and character of the excited states involved in the dynamics, we have monitored in each time step the electronic-density difference between the occupied excited state and the ground state for these two trajectories. This information is also plotted in Figure 3. Three types of electronic states are observed during the dynamics: localized, delocalized, and CT states.

In traj A, a localized state is initially populated (Figure 3). Within ∼50 fs, this high-energy exciton evolves into a *hot* CT state, which features a net electron−hole separation between the two monomers. This CT state persists up to ∼150 fs, remaining populated for 100 fs. After 150 fs, the low-lying states are populated and energy transfer occurs between the two bithiophene units, leading to an oscillation between localized and delocalized states, with no further sign of a CT state.

In traj B, the dynamics starts in a delocalized state. The intermolecular exciton localizes within 30 fs (Figure 3) and remains localized until the crossing to the ground state takes place. The radiationless deactivation mechanism to the ground state resembles that occurring in the bithiophene monomer: a ring-opening process.[56]

Role of the Ultrafast Nuclear Oscillations in the *Hot* Exciton Dynamics. The time-dependent evolution of the excited states is governed by ultrafast nuclear oscillations, namely: (i) CS vibrations (Figure 4), (ii) ring puckerings, and (iii) dihedral rotations ∠(SCCS). The time scales for processes i and ii are shorter than those for iii (50−100 vs 250−300 fs), making CS bond elongations and ring puckerings the major nuclear motions contributing to nonadiabatic relaxation. Here, we discuss the role of CS vibrations, being the most effective deactivation channel, while ring puckerings and dihedral rotations are addressed in Supplementary Note 3.

DOI: 10.1021/jacs.5b13210
J. Am. Chem. Soc. 2016, 138, 4502−4511

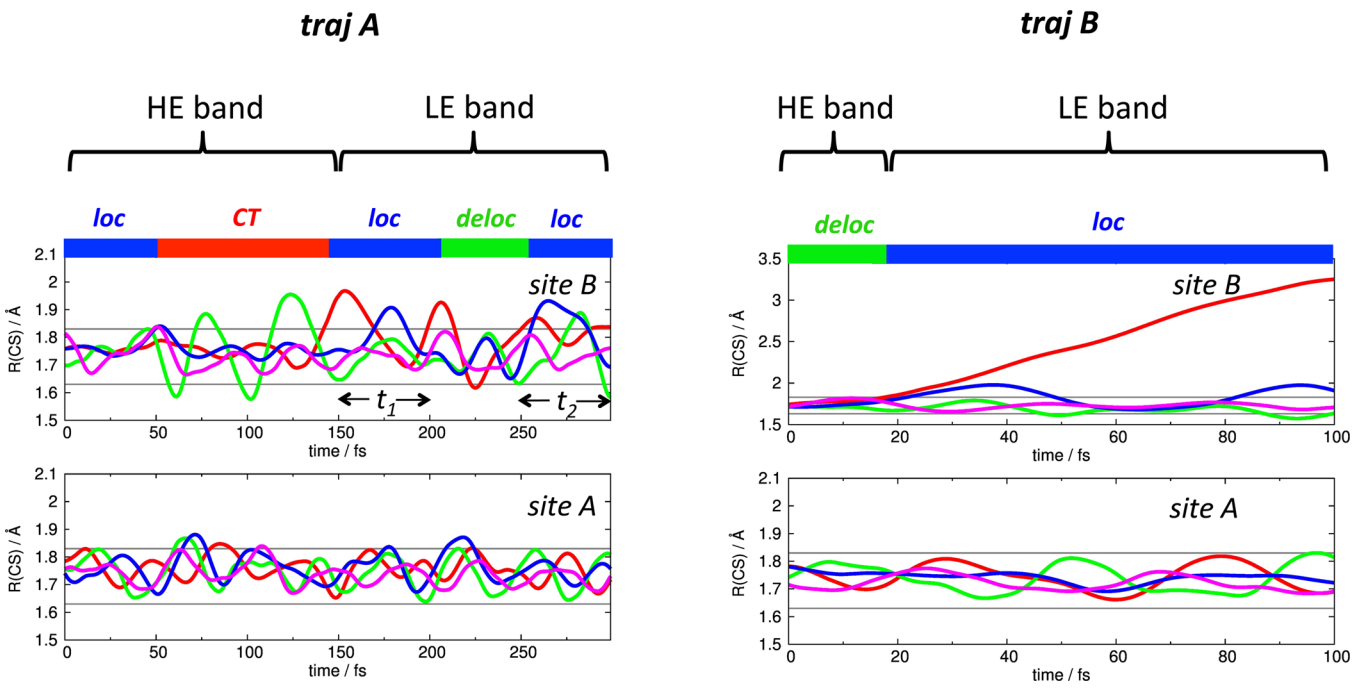

Figure 4. Variation of the CS distances in the bithiophene vdW dimer (molecular sites A and B) and classification of the occupied excited states during the nonadiabatic dynamics. Left, traj A (t = 0−300 fs); right, traj B (t = 0−100 fs). Gray lines: ⟨*BLAO*⟩ (see text).

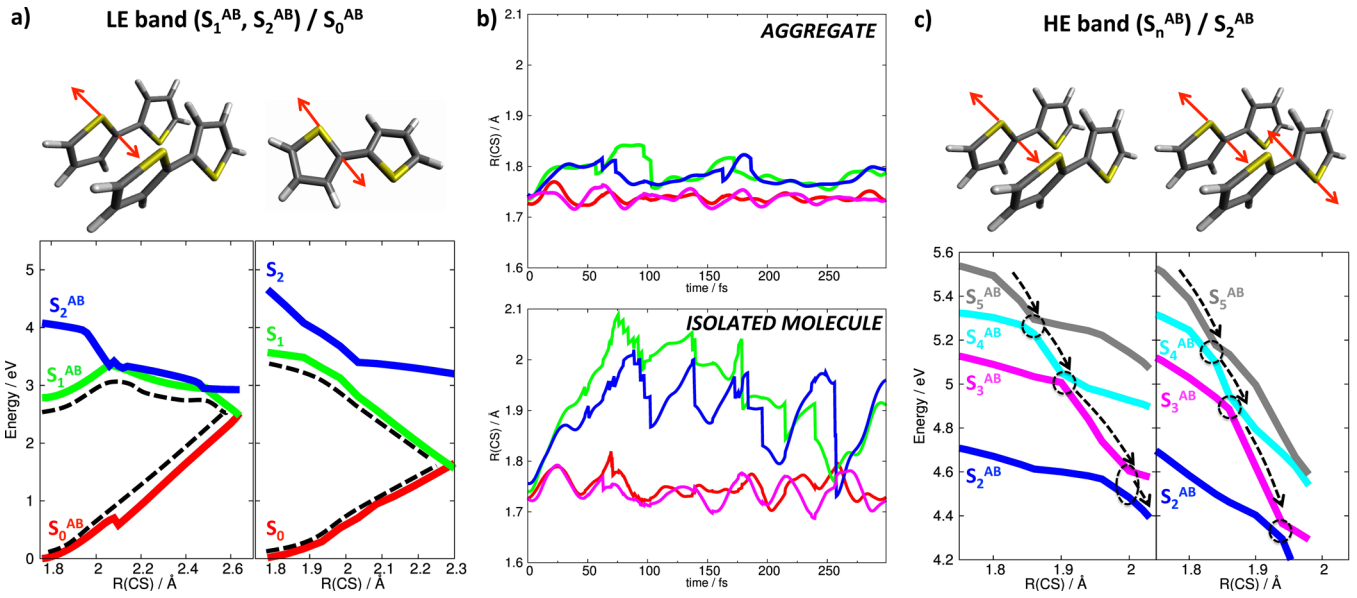

Figure 5. (a) TDDFT (ωB97XD/6-31G*) *relaxed* potential energy profiles of LE states (S_2^{AB}, S_1^{AB}) and ground state (S_0^{AB}) for the bithiophene dimer (left side). The profiles are computed by optimizing the S_1^{AB} state as a function of the CS distance (in increments of 0.02 Å) starting from the S_1^{AB} equilibrium structure; analogous curves are shown for the monomer at the right; dashed lines are meant to guide the eye. (b) Average CS distances for the bithiophene dimer (top) and monomer (bottom), as extracted from nonadiabatic excited-state dynamics; data for the monomer from ref 56. (c) *Single-point* TDDFT (ωB97XD/6-31G*) potential energy profiles of HE excited states (S_3^{AB}−S_5^{AB}) and S_2^{AB}, as a function of one CS distance in one bithiophene unit (left) or of two CS distances belonging to different molecular sites (right, dashed arrows to guide the eye).

For traj A, in the early stages of the relaxation process ($t \leq$ 150 fs), the CS stretchings control the ultrafast nonadiabatic transitions among high-lying excited states, bringing the dimer from the initial state (S_9^{AB}) to the *hot* CT state. Once the population is transferred from the *hot* CT to the LE band ($S_3^{AB} \rightarrow S_2^{AB}$, $t \sim$ 150 fs), exciton localization (intramolecular) and delocalization (intermolecular) processes occur (Figure 4). In the LE band, exciton localization tends to take place whenever the amplitude of a CS vibration is larger (smaller) than a quantity we call the *average Bond Length Amplitude Oscillation* (⟨*BLAO*⟩, gray horizontal lines in Figure 4). It is defined as $\langle BLAO \rangle = \langle BL \rangle \pm \Delta$, where $\langle BL \rangle$ is the average CS bond length, as computed at the equilibrium ground-state geometry of the dimer (S_0^{AB} state), and Δ is the average CS bond length fluctuation around $\langle BL \rangle$, as extracted from a 300 fs S_1 excited-state dynamics run of a single bithiophene molecule.[56] ⟨*BLAO*⟩ can be interpreted as an oscillation interval that allows us to decide whether exciton localization occurs (CS vibrations

DOI: 10.1021/jacs.5b13210
J. Am. Chem. Soc. 2016, 138, 4502−4511

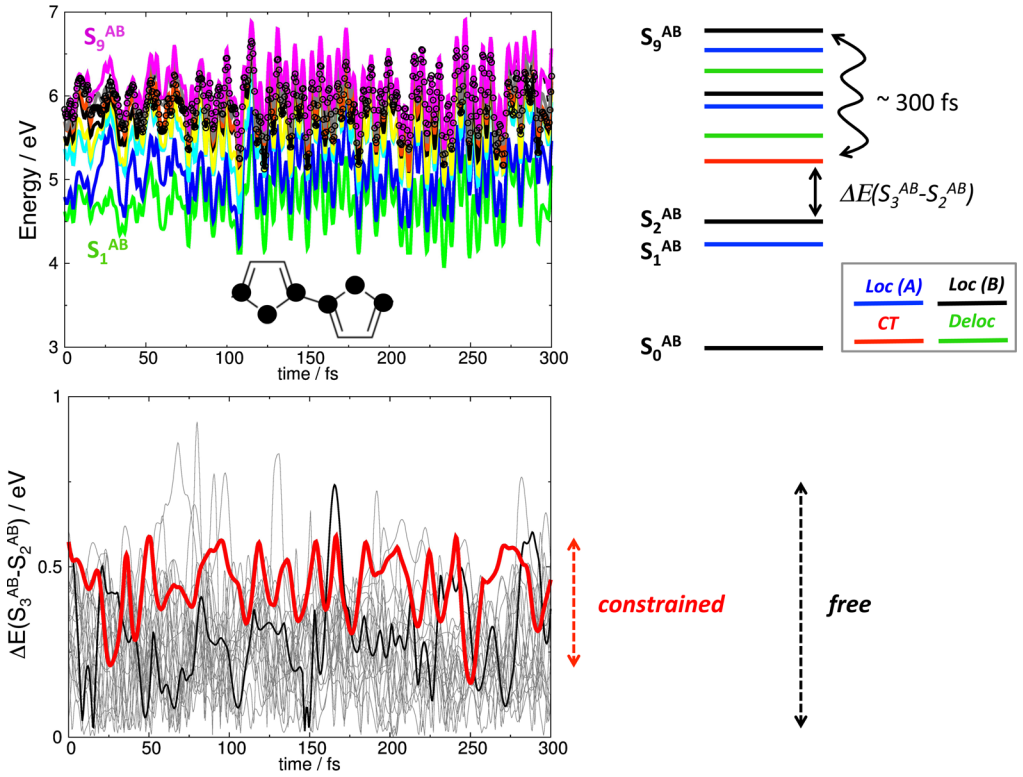

Figure 6. Top, left: TD-ωB97XD/6-31G* high-energy nonadiabatic excited state dynamics of a bithiophene dimer, for a trajectory with frozen Cartesian coordinates of some carbon and sulfur atoms (highlighted with black dots in the molecular structure). Top, right: sketch of the excited states involved in the deactivation process. Bottom: evolution of the gaps $\Delta E(S_3^{AB} - S_2^{AB})$ in all trajectories reaching the maximum simulation time in the unconstrained dynamics (gray lines), in the constrained trajectories with frozen coordinates (red line), and in trajectory A (black, see text).

beyond $\langle BLAO \rangle$ interval) or not (CS vibrations within $\langle BLAO \rangle$ interval), once the LE band is populated. At the ωB97XD/6-31G* level, $\langle BL \rangle$ = 1.73 Å and Δ = 0.1 Å.

In traj A, following the population of the LE band (~150 fs), exciton localization occurs in two time windows, 150 $\leq t_1 \leq$ 200 fs and $t_2 \geq$ 250 fs (Figure 4, left), when the amplitude of some CS vibrations is larger than $\langle BLAO \rangle$. For traj B, the CS bonds tend to oscillate between 1.6 and 2.0 Å (similar to traj A); however, at around 30 fs, one CS bond on molecular site B starts to strongly stretch (>2 Å), soon exceeding the upper limit of $\langle BLAO \rangle$ and continuing until it cleaves (Figure 4, right). This process leads to exciton localization and subsequent radiationless deactivation through the S_1^{AB}/S_0^{AB} crossing (Figure 3). The mechanism is similar to the $S_1 \rightarrow S_0$ nonradiative ring-opening pathway found for the isolated bithiophene monomer in ref 56.

The analysis of all trajectories reaching the maximum simulation time (without returning to the ground state) shows the same exciton dynamics as observed for traj A: (i) an initial decay (~20−50 fs) from high-lying excitons to *hot* CT states; (ii) survival and evolution of the *hot* CT states for ~50−100 fs; (iii) transfer to the low-lying excited states (S_2^{AB}, S_1^{AB}) originating from the structural breaking; and (iv) oscillations between localized and delocalized states in the LE regime, governed by CS vibrations.

The ultrafast population of *hot* CT states, as computed from our TDDFT nonadiabatic dynamics, matches well the experimental studies on a variety of organic materials,[4,18,21−23,32] which report formation of *hot* CTs within ~30−60 fs and further ultrafast photoinduced polaron generation.

We have already mentioned that the fraction of trajectories reaching the intersection with the ground state is much smaller in the dimer than in the monomer. The nonradiative pathways toward the ground state are controlled by CS bond stretchings, which destabilize the S_0 state and stabilize S_1.[56,60] Therefore, to understand the reason for the fewer radiationless processes in the dimer, we compare the excited-state potential energy profiles along the CS stretching and the average CS fluctuations in the monomer and in the dimer (Figure 5).

As shown in Figure 5a, the crossing between the S_1^{AB} state and the ground state is reached via an activated process in the dimer. From the S_1^{AB} minimum, a substantial potential energy barrier of ~0.5 eV needs to be overcome to reach this crossing. In the case of the bithiophene monomer, the process is barrierless instead. The barrier in the S_1^{AB} profile of the dimer impedes radiationless transitions to the ground state, which explains the slower return to the S_0^{AB} state, compared to the monomer.

The large difference between the reaction paths in the monomer and the dimer along the CS stretching coordinate is due to the energetics of the lowest $\pi\pi^*$ state in the region near the S_1 minimum (R(CS) < 2 Å). In the monomer, CS stretching lowers the energy of this state, whereas in the dimer it strongly raises the energy of the lowest $\pi\pi^*$ state by reducing the attractive intermolecular interactions. In both cases, CS stretching stabilizes the $\pi\sigma^*$ state. Consequently, in the monomer, the path in the lowest $\pi\pi^*$ state toward the crossing with the $\pi\sigma^*$ state (and eventually the ground state) is almost barrierless, while in the dimer there is a large barrier. Thus, the $\pi-\pi$ stacking interactions change the shape of the excited-state potential energy surfaces and ultimately govern the exciton

DOI: 10.1021/jacs.5b13210
J. Am. Chem. Soc. 2016, 138, 4502−4511

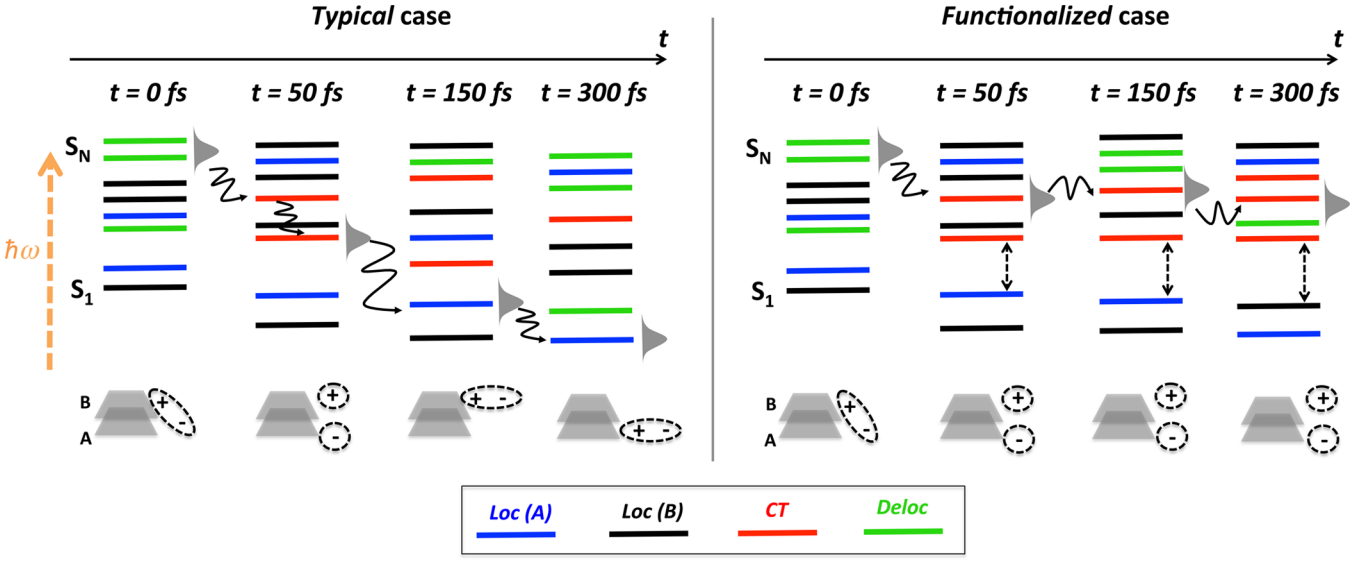

Figure 7. Schematic representation and classification of the excited states in an organic aggregate at different time steps during the excited-state dynamics. Left side: *typical* thiophene-based aggregate, with a sketch of the computed ultrafast deactivation via *hot* CT states. Right side: *functionalized* aggregate, with a sketch of the processes that tends to increase the lifetime of *hot* excitons (thus favoring CT processes) and to keep a high (≥0.2 eV) and constant energy gap $\Delta E(S_3^{AB} - S_2^{AB})$ (thus disfavoring exciton transfer to the LE regime).

dynamics,[61] as also indirectly observed via Raman spectroscopy in the case of oligothiophene aggregates.[62] Additional information on the energy profiles along the CS stretching coordinate is provided in the Supplementary Note 3 (Points 4 and 5).

As shown in Figure 5b, the mean CS bond length variations are smaller in the dimer (1.7 Å < R(CS) < 1.85 Å) than in the monomer (1.7 Å < R(CS) ≤ 2.1 Å), which lowers the chances of deactivation by the ring-opening mechanism. Thus, the S_1^{AB} potential energy barrier and the hindering of the CS oscillations in the dimer have the overall effect of increasing the lifetime of the low-energy excited states (e.g., S_2^{AB} and S_1^{AB}), lowering the odds of radiationless deactivation to the ground state.

The CS bond stretchings play another fundamental role even before the S_1^{AB} state is populated: they are ultimately responsible for driving the exciton relaxation through the HE band and on to the LE band. This is illustrated in the potential energy profiles from rigid scans shown in Figure 5c. These profiles were computed for two cases: (i) elongation of one CS bond (Figure 5c, left) from its equilibrium value (~1.72 Å) and (ii) concomitant stretching of two inner CS bonds belonging to different units (Figure 5c, right). Both motions destabilize the HE states and lead to state crossings that may act as funnels for exciton relaxation through the HE band and for the population of S_2^{AB} in the LE band.

The stabilization of S_3^{AB} leading to a state crossing with S_2^{AB} is of special interest. As discussed before (traj A), the $S_3^{AB} \rightarrow S_2^{AB}$ relaxation represents the population transfer from a *hot* CT state belonging to the HE band, to a localized state belonging to the LE band. The faster the $S_3^{AB} \rightarrow S_2^{AB}$ relaxation occurs, the shorter is the lifetime of *hot* CT states; and the lower is the probability of charge separation. As can be seen from Figure 5c, the stretching of the CS bonds governs the evolution of the S_3^{AB}–S_2^{AB} energy gap $\Delta E(S_3^{AB} - S_2^{AB})$, and thus the deactivation from HE to LE bands. Although we cannot exclude that S_2 may have CT character at some specific geometries, the data analysis shows that non-CT regions of the S_2 surface dominate the dynamics.

This gives rise to the following question: *Is there a way, by making use of design rules, to slow down the hot exciton deactivation processes, thus reducing the HE → LE relaxation and increasing the lifetime of high-energy states, which serve as a gateway to CT states?*

Design Rules for Long-Lived *Hot* CT States. A possible answer to the question above is suggested by additional TDDFT nonadiabatic dynamics simulations on the bithiophene dimer, in which the Cartesian coordinates of the sulfur atoms and the nearest bonded carbons are frozen, as indicated in Figure 6 (where only one bithiophene molecule is shown for clarity). In these constrained simulations (in which the C–H bonds and the C–C bonds in the thiophene ring are still free to oscillate), there are still ultrafast nonadiabatic transitions within the HE band, but those from the HE to the LE band are completely suppressed (Figure 6), as expected due to the artificial constraint on the CS distances. This supports our hypothesis that CS stretching vibrations are associated with the ultrafast relaxation within the manifold of excited states.

The exciton transfer from HE to LE is ruled by the energy gap $\Delta E(S_3^{AB} - S_2^{AB})$. In Figure 6 we compare the gaps obtained from the constrained dynamics (red line) and from all unconstrained trajectories reaching the maximum simulation time (gray lines). For the constrained dynamics, the computed gaps oscillate between 0.55 and 0.20 eV, while they vary over a much larger range in the unconstrained case, often reaching values as small as 0.01 eV. When the CS bond lengths are constrained, the $S_3^{AB} \rightarrow S_2^{AB}$ crossing is evidently inhibited, with a concomitant increase in the lifetime of the high-energy excited states in the HE band.

The simple intuitive design rule emerging from these restricted-dynamics simulations is that the lifetime of *hot* excitons[24,25] should be increased by finding ways to reduce the amplitude of the CS vibrations. Considering that the quantum oscillator amplitude is given by $(\hbar/\mu\omega)^{1/2}$, where μ is the reduced mass and ω the angular frequency, this could be achieved by increasing either μ or ω, for example by introducing into the molecular backbone isoelectronic heavy

DOI: 10.1021/jacs.5b13210
J. Am. Chem. Soc. 2016, 138, 4502–4511

atoms (e.g., Se vs S, or Si vs C as recently reported,[63] increase in μ), or fused thiophene rings which flatten the structure and enhance the local C−S electron density (e.g., thienoacene units, increase in ω). We note that these chemical modifications are motivated only by qualitative arguments and that we do not yet have any computational data to support them. Moreover, they focus exclusively on the control of the nuclear vibrations, without considering their impact on the electronic structure.

In Figure 7 (left side), we schematically sketch and summarize our findings. For (*typical*) thiophene-based aggregates, the initial high-energy exciton evolves via nonadiabatic transitions to *hot* CT states that are populated in tens of femtoseconds. *Hot* CT states last for ∼100 fs, and then decay to low-lying excited states. At the bottom of the excited-state LE band, the exciton oscillates between localized and delocalized states without ever returning to a CT state. For a hypothetical *functionalized* aggregate where the HE and LE bands are kept energetically apart (Figure 7 right side), the exciton is trapped in the HE band and does not populate the LE band (on an ultrafast time scale), which would increase the probability of populating CT states.

The readjustment of the electronic structure due to repopulation of excited states favoring specific relaxation channels resembles the so-called *shishiodoshi* transfer mechanism, which denotes a concerted unidirectional electronic and vibrational energy transfer through a chain of excited states with descending energy; this process is enhanced by vibronic relaxations.[7]

The ultrafast decay via *hot* CT states, observed in our full-dimensional TDDFT nonadiabatic dynamics, has important consequences for thiophene-based homo- and heterogeneous organic interfaces used for electronic and photovoltaic applications. The possibility of populating in few femtoseconds a high-energy CT state that may live over longer times opens the way for ultrafast electron transfer and charge separation, before relaxation to the bottom of the interfacial excited states can happen.

CONCLUSIONS

Full-dimensional nonadiabatic excited-state dynamics based on linear-response TDDFT allow us to gain insight into the photophysics of high-energy (*hot*) excitons at organic/organic interfaces. Ultrafast exciton deactivation processes were investigated for a bithiophene dimer, considered as representative of a large class of molecular aggregates, homogeneous and heterogeneous organic interfaces. The time scales and relaxation processes emerging from our TDDFT simulations nicely agree with data from state-of-the-art ultrafast spectroscopy on small thiophene-based conjugated molecules, acenes, homo- and copolymers, and even on polymer/fullerene interfaces.[22,25,26,32,64−68] These findings are of general relevance for the interpretation and understanding of ultrafast excitonic processes in functional conjugated molecular aggregates, and for the design of new efficient solid-state photoactive materials.

In the early stages of the relaxation process (∼20−50 fs), ultrafast nonadiabatic transitions occur within the manifold of high-energy excited states, populating *hot* CT states. *Hot* CTs live for ∼100 fs and then decay to low-energy states, namely S_2^{AB} and S_1^{AB}. Thereafter, the system oscillates between localized and delocalized states, in a process governed by CS vibrations. Already at 300 fs, 80% of the occupation is transferred to the bottom of the excited-state manifold, from where nonradiative decay processes through S_1/S_0 crossings occur, but much less frequently than in the monomer case.[56,59] This can be traced back to an energy barrier between the S_1 minimum and the S_1/S_0 crossing, which impedes nonradiative S_1/S_0 deactivation in the vdW dimer.

Nonadiabatic transitions within the manifold of the excited states are fostered by CS vibrations. CS bond elongations stabilize the excited states, thus promoting fast depopulation of *hot* CT states and reducing the energy gap between HE and LE bands (via pronounced stabilization of the S_3 state).

Increasing the lifetime of *hot* excitons is a possible way to enhance the occupation of the CT states, which may lead to polaron formation in molecular aggregates. We explored this possibility by running constrained nonadiabatic excited-state dynamics, in which the promoting CS vibrations were suppressed by freezing the corresponding coordinates. This prevented the ultrafast population of low-lying excited states (Figure 6), without inhibiting nonadiabatic transitions within the high-energy excited-state manifold. The resulting increase in the lifetime of *hot* excitons improves the odds of populating long-lived *hot* CT states (Figure 7).

On the basis of these findings, we conclude that the search for ways to extend *hot*-exciton lifetimes may be a productive goal in the design of molecular aggregates for photovoltaics. For example, focusing on the mechanics of the nuclear frame, we anticipate that replacement of Se for S (or maybe Si for C) in the molecular backbone may mechanically reduce the amplitude of the relevant promoting vibrations and that introduction of fused thiophene rings (e.g., thienoacene units)[69] may lead to a higher electron density in the CS bonds and strengthen them; these measures may increase the lifetime of *hot* excitons and open an energy gap between the HE and LE bands, thus impeding nonadiabatic HE−LE transitions (with localization and recombination). However, we note that these measures will also impact the electronic structure, in ways that we have not yet evaluated.

Independently of the success of such heuristic approaches, we emphasize that the bithiophene dimer investigated in this work should be understood as a prototype for photoinduced charge-separation in vdW organic dimers. Although it is gratifying that our simulations agree with the measured photoinduced charge transfer time constants in organic crystals and semiconducting polymers, we believe that the most interesting aspect of our study is the demonstration of how the first-principles characterization of the time evolution of the electronic structure may lead to new insights on molecular design. Rather than expecting larger complexes to share the same electronic features as our small prototype, we believe that the goal should be the following: given a certain organic crystal, we should identify and locate the CT states within the manifold of the electronically excited states relevant to ultrafast relaxation, and then try to devise ways to increase their lifetime by isolating them at the bottom of the electronic band. We believe that this approach is a true step forward in relation to the common analysis based on HOMO−LUMO gaps and vertical excitation spectra.

Future work will need to focus on the investigation of singlet-state dynamics in larger molecular aggregates and at donor/acceptor interfaces[32] and on singlet−triplet exciton dynamics.[70] This will require nonadiabatic excited-state dynamics simulations with theoretical methods, such as linear response TDDFT, that are able to *reasonably* describe the excited-state electronic structure[39,71] of medium−large systems.

DOI: 10.1021/jacs.5b13210
J. Am. Chem. Soc. 2016, 138, 4502−4511

■ ASSOCIATED CONTENT

Supporting Information

The Supporting Information is available free of charge on the ACS Publications website at DOI: 10.1021/jacs.5b13210.

Supplementary Note 1: ground state optimized geometries, excited state (singlet and triplet) vertical transition energies, double excitations, and absorption spectra. Supplementary Note 2: details on the computational methods and fitting procedure for the HE and LE state population. Supplementary Note 3: time-dependent oscillations of internal coordinates (ring puckering, C−C bond length and bithiophene dihedral angle oscillations); electron densities evaluated along traj A, traj B and trajectory with frozen degrees of freedom; energy of the triplet states along the dynamics; and S_1 relaxed potential energy profiles for different values of the intermolecular dimer distance. Supplementary Note 4: optimized Cartesian coordinates and absolute energies (PDF)

■ AUTHOR INFORMATION

Corresponding Authors

*fazzi@kofo.mpg.de
*mario.barbatti@univ-amu.fr
*thiel@kofo.mpg.de

Notes

The authors declare no competing financial interest.

■ ACKNOWLEDGMENTS

D.F. acknowledges the Alexander von Humboldt foundation for a postdoctoral research fellowship. M.B. thanks the support from the A*MIDEX grant (No. ANR-11-IDEX-0001-02) and from the project Equip@Meso (ANR-10-EQPX-29-01), both funded by the French Government Investissements d'Avenir program.

■ REFERENCES

(1) Zewail, A. H. *J. Phys. Chem. A* **2000**, *104*, 5660.
(2) Long, R.; Prezhdo, O. V. *Nano Lett.* **2014**, *14*, 3335.
(3) Junhyeok Bang, S. M.; Sun, Y.-Y.; West, D.; Wang, Z.; Gao, F.; Zhang, S. B. *Proc. Natl. Acad. Sci. U. S. A.* **2013**, *110*, 908.
(4) Oldani, N.; Tretiak, S.; Bazan, G.; Fernandez-Alberti, S. *Energy Environ. Sci.* **2014**, *7*, 1175.
(5) Gregory, D.; Scholes, G. R. *Nat. Mater.* **2006**, *5*, 14.
(6) Collini, E. *Chem. Soc. Rev.* **2013**, *42*, 4932.
(7) Nelson, T.; Fernandez-Alberti, S.; Roitberg, A. E.; Tretiak, S. *Acc. Chem. Res.* **2014**, *47*, 1155.
(8) Collini, E.; Scholes, G. D. *Science* **2009**, *323*, 369.
(9) Watanabe, S.; Ando, K.; Kang, K.; Mooser, S.; Vaynzof, Y.; Kurebayashi, H.; Saitoh, E.; Sirringhaus, H. *Nat. Phys.* **2014**, *10*, 308.
(10) Akimov, A. V.; Neukirch, A. J.; Prezhdo, O. V. *Chem. Rev.* **2013**, *113*, 4496.
(11) Clarke, T. M.; Durrant, J. R. *Chem. Rev.* **2010**, *110*, 6736.
(12) Brédas, J.-L.; Norton, J. E.; Cornil, Je.; Coropceanu, V. *Acc. Chem. Res.* **2009**, *42*, 1691.
(13) Clark, J.; Nelson, T.; Tretiak, S.; Cirmi, G.; Lanzani, G. *Nat. Phys.* **2012**, *8*, 225.
(14) Bubnova, O.; Khan, Z. U.; Wang, H.; Braun, S.; Evans, D. R.; Fabretto, M.; Hojati-Talemi, P.; Dagnelund, D.; Arlin, J. B.; Geerts, Y. H.; Desbief, S.; Breiby, D. W.; Andreasen, J. W.; Lazzaroni, R.; Chen, W. M.; Zozoulenko, I.; Fahlman, M.; Murphy, P. J.; Berggren, M.; Crispin, X. *Nat. Mater.* **2014**, *13*, 190.
(15) Akselrod, G. M.; Deotare, P. B.; Thompson, N. J.; Lee, J.; Tisdale, W. A.; Baldo, M. A.; Menon, V. M.; Bulovic, V. *Nat. Commun.* **2014**, *5*, 3646.
(16) Noriega, R.; Rivnay, J.; Vandewal, K.; Koch, F. P.; Stingelin, N.; Smith, P.; Toney, M. F.; Salleo, A. *Nat. Mater.* **2013**, *12*, 1038.
(17) Song, Y.; Clafton, S. N.; Pensack, R. D.; Kee, T. W.; Scholes, G. D. *Nat. Commun.* **2014**, *5*, 4933.
(18) Provencher, F.; Berube, N.; Parker, A. W.; Greetham, G. M.; Towrie, M.; Hellmann, C.; Cote, M.; Stingelin, N.; Silva, C.; Hayes, S. C. *Nat. Commun.* **2014**, *5*, 4288.
(19) Vázquez, H.; Troisi, A. *Phys. Rev. B: Condens. Matter Mater. Phys.* **2013**, *88*, 205304.
(20) Bera, S.; Gheeraert, N.; Fratini, S.; Ciuchi, S.; Florens, S. *Phys. Rev. B: Condens. Matter Mater. Phys.* **2015**, *91*, 041107.
(21) Gelinas, S.; Rao, A.; Kumar, A.; Smith, S. L.; Chin, A. W.; Clark, J.; van der Poll, T. S.; Bazan, G. C.; Friend, R. H. *Science* **2014**, *343*, 512.
(22) Najafov, H.; Lyu, B.; Biaggio, I.; Podzorov, V. *Phys. Rev. B: Condens. Matter Mater. Phys.* **2008**, *77*, 125202.
(23) Guo, J.; Ohkita, H.; Benten, H.; Ito, S. *J. Am. Chem. Soc.* **2009**, *131*, 16869.
(24) Grancini, G.; Maiuri, M.; Fazzi, D.; Petrozza, A.; Egelhaaf, H. J.; Brida, D.; Cerullo, G.; Lanzani, G. *Nat. Mater.* **2013**, *12*, 29.
(25) Bakulin, A. A.; Rao, A.; Pavelyev, V. G.; van Loosdrecht, P. H.; Pshenichnikov, M. S.; Niedzialek, D.; Cornil, J.; Beljonne, D.; Friend, R. H. *Science* **2012**, *335*, 1340.
(26) Paraecattil, A. A.; Banerji, N. *J. Am. Chem. Soc.* **2014**, *136*, 1472.
(27) Banerji, N. *J. Mater. Chem. C* **2013**, *1*, 3052.
(28) Moses, D. *Nat. Mater.* **2014**, *13*, 4.
(29) Tavernelli, I. *Acc. Chem. Res.* **2015**, *48*, 792.
(30) Wang, L.; Long, R.; Prezhdo, O. V. *Annu. Rev. Phys. Chem.* **2015**, *66*, 549.
(31) Sterpone, F.; Rossky, P. J. *J. Phys. Chem. B* **2008**, *112* (16), 4983.
(32) Jailaubekov, A. E.; Willard, A. P.; Tritsch, J. R.; Chan, W. L.; Sai, N.; Gearba, R.; Kaake, L. G.; Williams, K. J.; Leung, K.; Rossky, P. J.; Zhu, X. Y. *Nat. Mater.* **2013**, *12*, 66.
(33) Tamura, H.; Bittner, E. R.; Burghardt, I. *J. Chem. Phys.* **2007**, *126*, 021103.
(34) Tamura, H.; Burghardt, I. *J. Am. Chem. Soc.* **2013**, *135*, 16364.
(35) Nelson, T.; Fernandez-Alberti, S.; Chernyak, V.; Roitberg, A. E.; Tretiak, S. *J. Phys. Chem. B* **2011**, *115*, 5402.
(36) Wang, L.; Prezhdo, O. V.; Beljonne, D. *Phys. Chem. Chem. Phys.* **2015**, *17*, 12395.
(37) Liu, J.; Neukirch, A. J.; Prezhdo, O. V. *J. Phys. Chem. C* **2014**, *118*, 20702.
(38) Tapavicza, E.; Bellchambers, G. D.; Vincent, J. C.; Furche, F. *Phys. Chem. Chem. Phys.* **2013**, *15*, 18336.
(39) Sen, K.; Crespo-Otero, R.; Weingart, O.; Thiel, W.; Barbatti, M. *J. Chem. Theory Comput.* **2013**, *9*, 533.
(40) Caruso, D.; Troisi, A. *Proc. Natl. Acad. Sci. U. S. A.* **2012**, *109*, 13498.
(41) Dreuw, A.; Wormit, M. *WIREs Comput. Mol. Sci.* **2015**, *5*, 82.
(42) Barbatti, M.; Ruckenbauer, M.; Plasser, F.; Pittner, J.; Granucci, G.; Persico, M.; Lischka, H. *WIREs Comput. Mol. Sci.* **2014**, *4*, 26.
(43) Granucci, G.; Persico, M. *J. Chem. Phys.* **2007**, *126*, 134114.
(44) Fernandez-Alberti, S.; Roitberg, A. E.; Nelson, T.; Tretiak, S. *J. Chem. Phys.* **2012**, *137*, 014512.
(45) Wang, L.; Prezhdo, O. V. *J. Phys. Chem. Lett.* **2014**, *5*, 713.
(46) Granucci, G.; Persico, M.; Toniolo, A. *J. Chem. Phys.* **2001**, *114*, 10608.
(47) Plasser, F.; Granucci, G.; Pittner, J.; Barbatti, M.; Persico, M.; Lischka, H. *J. Chem. Phys.* **2012**, *137*, 22A514.
(48) Wang, L.; Beljonne, D. *J. Phys. Chem. Lett.* **2013**, *4*, 1888.
(49) Wang, L.; Trivedi, D.; Prezhdo, O. V. *J. Chem. Theory Comput.* **2014**, *10*, 3598.
(50) Hammes-Schiffer, S.; Tully, J. C. *J. Chem. Phys.* **1994**, *101*, 4657.
(51) Casida, M. In *Recent Advances in Density Functional Methods, Part I*; Chong, D., Ed.; World Scientific: Singapore, 1995; p 155.
(52) Barbatti, M.; Pittner, J.; Pederzoli, M.; Werner, U.; Mitrić, R.; Bonačić-Koutecký, V.; Lischka, H. *Chem. Phys.* **2010**, *375*, 26.

DOI: 10.1021/jacs.5b13210
J. Am. Chem. Soc. 2016, 138, 4502−4511

(53) Mališ, M.; Loquais, Y.; Gloaguen, E.; Biswal, H. S.; Piuzzi, F.; Tardivel, B.; Brenner, V.; Broquier, M.; Jouvet, C.; Mons, M.; Došlić, N.; Ljubić, I. *J. Am. Chem. Soc.* **2012**, *134*, 20340.
(54) Werner, U.; Mitrić, R.; Suzuki, T.; Bonačić-Koutecký, V. *Chem. Phys.* **2008**, *349*, 319.
(55) Tapavicza, E.; Tavernelli, I.; Rothlisberger, U. *Phys. Rev. Lett.* **2007**, *98*, 023001.
(56) Fazzi, D.; Barbatti, M.; Thiel, W. *Phys. Chem. Chem. Phys.* **2015**, *17*, 7787.
(57) Crespo-Otero, R.; Barbatti, M. *Theor. Chem. Acc.* **2012**, *131*, 1237.
(58) Schnell, M.; Erlekam, U.; Bunker, P. R.; von Helden, G.; Grabow, J.-U.; Meijer, G.; van der Avoird, A. *Angew. Chem., Int. Ed.* **2013**, *52*, 5180.
(59) Prlj, A.; Curchod, B. F.; Corminboeuf, C. *Phys. Chem. Chem. Phys.* **2015**, *17*, 14719.
(60) Weinkauf, R.; Lehr, L.; Schlag, E. W.; Salzmann, S.; Marian, C. M. *Phys. Chem. Chem. Phys.* **2008**, *10*, 393.
(61) Settels, V.; Schubert, A.; Tafipolski, M.; Liu, W.; Stehr, V.; Topczak, A. K.; Pflaum, J.; Deibel, C.; Fink, R. F.; Engel, V.; Engels, B. *J. Am. Chem. Soc.* **2014**, *136*, 9327.
(62) Milani, A.; Brambilla, L.; Del Zoppo, M.; Zerbi, G. *J. Phys. Chem. B* **2007**, *111*, 1271.
(63) Li, L.; Matsuo, T.; Hashizume, D.; Fueno, H.; Tanaka, K.; Tamao, K. *J. Am. Chem. Soc.* **2015**, *137*, 15026.
(64) Fazzi, D.; Grancini, G.; Maiuri, M.; Brida, D.; Cerullo, G.; Lanzani, G. *Phys. Chem. Chem. Phys.* **2012**, *14*, 6367.
(65) Hwang, I.; Beaupré, S.; Leclerc, M.; Scholes, G. D. *Chem. Sci.* **2012**, *3*, 2270.
(66) Vandewal, K.; Albrecht, S.; Hoke, E. T.; Graham, K. R.; Widmer, J.; Douglas, J. D.; Schubert, M.; Mateker, W. R.; Bloking, J. T.; Burkhard, G. F.; Sellinger, A.; Frechet, J. M.; Amassian, A.; Riede, M. K.; McGehee, M. D.; Neher, D.; Salleo, A. *Nat. Mater.* **2014**, *13*, 63.
(67) Banerji, N.; Gagnon, E.; Morgantini, P.-Y.; Valouch, S.; Mohebbi, A. R.; Seo, J.-H.; Leclerc, M.; Heeger, A. J. *J. Phys. Chem. C* **2012**, *116*, 11456.
(68) Scarongella, M.; Laktionov, A.; Rothlisberger, U.; Banerji, N. *J. Mater. Chem. C* **2013**, *1*, 2308.
(69) Cinar, M. E.; Ozturk, T. *Chem. Rev.* **2015**, *115*, 3036.
(70) Cui, G.; Thiel, W. *J. Chem. Phys.* **2014**, *141*, 124101.
(71) Laurent, A. D.; Jacquemin, D. *Int. J. Quantum Chem.* **2013**, *113*, 2019.

DOI: 10.1021/jacs.5b13210
J. Am. Chem. Soc. 2016, 138, 4502−4511